CURE-ON-D

Ultra-High-Solid Nonskid Coatings

Through Frontal Polymerization

DANIEL P. GARY, DOUGLAS NGO, AMBER BUI, JORGE A. BELGODERE, AND JOHN A. POJMAN / Louisiana State University

Current two-component coatings require exact mixing ratios for application and performance, have varying cure times, and release volatile organic compounds (VOCs). Cure-on-demand technology can be used to combat these challenges.

This technology includes photocuring based on acrylate and epoxy-based resins.[1–5] Photocuring can be used to cure coatings rapidly, but the inner filter effect limits the through-cure of thick samples. In addition to thickness, the presence of fillers or pigments impedes light penetration, thereby reducing the cure of the material.[6] Such challenges can make photocuring a difficult process in the curing of nonskid coatings, which are often thick and highly filled. A post-thermal cure is a potential way to overcome this issue, but it requires additional time and resources.[7] Redox-initiated polymerization can be used to rapidly prepare materials such as coatings and composites without the drawback of the inner filter effect.[8–11]

EMAND,

However, the pot life is limited, and two-part mixing is required.[11]

Frontal polymerization (FP) is a potential method that can be used to rapidly cure a highly filled or thick coating without the drawbacks of photocuring and redox polymerization. Frontal polymerization was first discovered by Chechilo and Enikolopyan in the 1970s[12–15] and then was independently discovered by Pojman in the early 1990s.[16–22] Since its discovery, FP research has been extended to other areas such as deep eutectic solvents,[23–26] hydrogels,[27] gradient materials,[28] cationic-initiated polymerization,[29–33] and ring-opening metathesis polymerization.[34–36]

More recently, Bansal et al. demonstrated the first use of FP to make coatings on wooden substrates.[37] However, FP has not been used to manufacture coatings on steel substrates. One of the drawbacks of FP is heat loss to the substrate, which can be exacerbated by the high thermal conductivity of materials such as steel. Because of this, it is difficult to maintain a front without continuous input of energy. In addition, buoyancy-driven convection from the density difference between the formed polymer and resin increases heat loss that can quench the front.[38] Adding fillers to form a moldable putty is one way to eliminate buoyancy-driven convection;[39] however, the presence of fillers also results in front temperature reduction.[40]

Herein, we utilize the process of frontal polymerization to rapidly cure a cure-on-demand, nonskid, one-pot coating formulation for maritime usage. Unlike traditional FP, where the front self-propagates after initiation, here the coating is continuously irradiated with an infrared heater to sustain the front propagation. A base formulation consisting of Ebecryl®605 (73 wt % bisphenol-A epoxy acrylate diluted with 27 wt % tripropylene glycol diacrylate) and pentaerythritol triacrylate (PETIA) was used as the resin. Ebecryl®605 was chosen to impart adhesion to the epoxy primer and provide barrier properties. PETIA, a 1:1 mixture of tri- and tetra-acrylate, was used as a reactive diluent to reduce cure time, increase

FIGURE 1
Structures of (1) bisphenol-A epoxy acrylate, (2) 1,1-bis(tert-butyl-peroxy)-3,3,5-tricyclohexane, (3) tripropylene glycol diacrylate, and (4) pentaerythritol triacrylate.

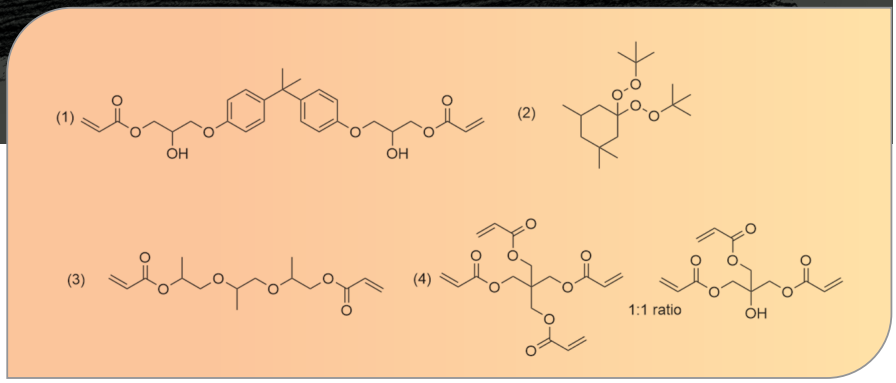

crosslink density, and maintain adhesion. Fumed silica was added to suppress buoyancy-driven connection. Zoltek®PX35 is a high-aspect ratio milled carbon-fiber filler used to reduce cracking from thermal stresses. The high crosslink density and choice of fillers minimize cure time and help provide a barrier against chemicals and corrosion. All materials were used as received. **Figure 1** shows the chemical structures of the initiator and resins.

EXPERIMENTAL

Materials

- Ebecryl®605 and pentaerythritol triacrylate (PETIA) were purchased from allnex (Alpharetta, GA).
- 1,1-*bis*(*tert*-butylperoxy)-3,3,5-tricyclohexane (Luperox®231) was obtained from Sigma Aldrich.
- Fumed silica (Aerosil®200, 175 – 225 m^2/g BET surface area) was obtained from Evonik Industries (Parsippany, NJ).
- Zoltek®PX35 (referred to as Zoltek or milled carbon fiber, 150 x 7.2 squared microns) was provided by Zoltek Companies, Inc. (St. Louis, MO).
- Aluminum oxide (16 grit, 14 mesh, 1.2 mm) was obtained from Floorguard Products, Inc. (Aurora, IL).
- Polygloss®90 (a kaolinite clay referred to as kaolin, 0.4 microns) was obtained from KaMin performance minerals (Macon, GA).
- Hubercarb®Q3 (calcium carbonate, 3.2 microns median particle size) was purchased from Huber Materials (Quincy, IL).
- Natural seawater was obtained from the Gulf of Mexico (Gulf Shores, AL).
- Synthetic seawater (following ASTM D1141) was obtained from Grainger (Arlington, TX). Skilcraft®1064006 (non-ionic liquid detergent) was purchased from SkyGeek (LaGrangeville, NY).
- Ethanol (200 proof) was purchased from Koptek (King of Prussia, PA).

FIGURE 2
General setup for experiments.

- Castrol®GTX High Mileage (synthetic motor oil) was purchased from BP Lubricants USA, Inc. (Wayne, NJ).
- AVL-TKS anti-icing deicing fluid was purchased from Aviation Laboratories, Inc. (Houston, TX).

Addition of Fumed Silica to Reduce Cure Time

A resin blend (10 g) consisting of Ebecryl®605 (60 wt %) and PETIA (40 wt %) was prepared, and one parts per hundred resin (phr) of Luperox®231 was added to it. Phr refers to the amount of material added (in grams) for every 100 grams of resin. Various amounts of fumed silica were then added (0 to 5 phr). The formulations were mixed after the addition of each component. 6" x 4" x 1/8" steel panels coated with an epoxy primer (Interbond®998, from International Paint) were used as the substrates. The panels were previously primed, and all coatings in this work were applied after the overcoat window. The panels were sanded down using 60 grit sandpaper and then cleaned with ethanol before coating application. All surface preparation in this manuscript was done as just described. A drawdown bar (10 cm x 2 cm) was used to apply the coatings at a wet film thickness of 1000 µm (40 mils). Curing was initiated using an infrared Solary®1R1 heater (1100 W, 15" x 2.75") positioned 10 cm (4") above the coating. **Figure 2** shows the general experimental setup. Temperatures were recorded using an infrared thermometer, NUB®8500H, with the laser pointed towards the center of the coating surface from a distance of approximately 10 cm. A stopwatch was used to record time. There is an apparent color change when the coating is done curing; each coating was probed to ensure that no unreacted formulation remained.

Fillers as Additives to Reduce Internal Stresses and Prevent Cracking

The resin and initiator were added as previously mentioned. The filler (milled carbon fiber, kaolin, or calcium carbonate) was added, and the formulation was then applied and cured. For the milled carbon-fiber formulations, the fillers were added in increments of 5 phr. Twenty phr of filler was added for the kaolin and calcium carbonate-containing formulations. Fumed silica (5 phr) was then added to each formulation. The formulations were stirred after the addition of each component.

Wet Film Thickness Study

The resin and initiator were added as described earlier. Fumed silica (5 phr) was then added, and the formulation was mixed. The wet film thickness was controlled using a drawdown bar and varied from 250 µm to 1000 µm (10–40 mils).

Resin Composition Study

The composition of the resin mixture varied from 0 wt % to 100 wt % PETIA or Ebecryl®605. Fumed silica (5 phr) was added and then the formulation was mixed. The coatings were then applied (40 mils) and cured as previously mentioned.

Varying the Distance of Heat Source

The distance between the infrared heater and panel was varied from 2 inches (5 cm) to 8 inches (20 cm). For these experiments, a resin blend of Ebecryl®605 (60 wt %) and PETIA (40 wt %) was prepared, and Luperox®231 (1 phr) was added. Fumed silica (5 phr) was added last and the formulations were mixed. Each coating was applied to the panel at a wet film thickness of 40 mils with a drawdown bar.

FIGURE 3
Impact sequence for the impact test. (From bottom up and then left to right.)

2	5	11	7	3
6	19	23	20	16
10	22	25	24	12
14	18	21	17	8
1	5	9	13	4

Preparation of Nonskid Coatings

A resin blend consisting of Ebecryl®605 (60 wt %) and PETIA (40 wt %) was prepared, and 1 phr of Luperox®231 was added. The amount of blend prepared depended on the size of the substrate area to be coated. Eleven grams of resin was used for a 6" x 3" area, 15 g of resin was used for a 6" x 4" area, 22.5 g for a 6" x 6" area, and 90 g for a 12" x 12" area. Milled carbon fiber (20 phr) was added followed by fumed silica (5 phr). Initially, 100 phr of aluminum oxide was added (the preliminary nonskid); this was later reduced to 25 phr. The formulations were mixed after the addition of each component. Each substrate was primed with Interbond®998 and sanded down as previously described. The coating with 25 phr of aluminum oxide was applied on the substrate using a fiberglass aluminum alloy roller (11 inches total length). The roller (3" x 0.75") had grooves measuring 1 mm deep. The preliminary nonskid was applied by a 2-inch flat-edge paintbrush onto a 6" x 4" x 1/8" primed panel. In the preparation of the nonskid for impact testing, the temperature of the uncoated substrate is measured. A stopwatch was used to record the time, and the curing of the coating was apparent with a color change. Each coating was probed to ensure that no unreacted formulation remained. The mass change of the resin between the wet and cured state was determined for the preliminary nonskid.

Impact Testing

Impact testing was done following ASTM G14. A 4-lb weight was dropped onto an indenter punch resting on the coated panel. For each impact test, a total of 25 impacts were made in a 3" x 3" area using the sequence shown in **Figure 3**. A 1-inch chisel was then used to remove any loosened nonskid coating around the impact zone. The number of connections between adjacent impacts was counted. The score was determined by multiplying the sum of these connections by 2.5 and then subtracting from 100. The total score reflects the percentage of intact coating remaining in between the impact sites. The coating formulation was applied in a 6" x 6" area (half of the panel area) on a 12" x 6" x 1/8" primed panel. Two nonskid samples were impacted without treatment, and four were impacted after treatment with synthetic seawater for 15 days in accordance with ASTM D1141.

Chemical Testing

Qualitative chemical testing was done to determine the relative resistance of the nonskid to various chemicals including ethanol, natural saltwater, motor oil, detergent, and deicing-defrosting fluid. For each test, two nonskid coatings were prepared (see the Preparation of Nonskid Coatings section for details) on 6" x 4" x 1/8" primed steel panels. One nonskid was impacted twice, with the impacts being 4 inches apart from each other and 1 inch from the edges. Each nonskid coating was placed in a beaker (1500 mL) and halfway submerged in each chemical; the beakers were then sealed with foil. The nonskid coatings were then submerged in one of the following: ethanol (24 hours), deicing-defrosting fluid (24 hours), and for 4 weeks in seawater, motor oil, or detergent. After removal, each

nonskid panel was probed with a 1-inch chisel to determine loss of adhesion or softening of the coating. The unsubmerged and submerged parts were compared along with the impacted versus nonimpacted coating. The coatings submerged in ethanol and deicing-defrosting fluid were given a 6-hour recovery period before evaluation.

Corrosion Testing

A salt-fog test was done to test corrosion resistance. Two abrasive blasted steel test panels (3–4 mils) were coated with Interbond®998 (a qualified MIL-PRF-23236 Type VII coating). The panels were 12" x 12" x 1/8" (304.8 x 304.8 x 3.17 millimeters). A 5 ¾" x ¼" (145 x 6 millimeter) (nominal) linear scribe in the nonskid system was cut to the bare steel using a drill bit and drill press. The two samples were subjected to accelerated corrosion for 1000 hours in a salt-fog cabinet in accordance with ASTM B1170. Upon completion of the accelerated corrosion exposure, the samples were removed from the salt-fog cabinet, rinsed in potable water, and dried with lint-free laboratory wipes. Immediately after the residual rinse water was removed, the scribe area of each panel was prepared and inspected in accordance with ASTM D1654 for separation between layers, loss of adhesion, undercutting, and corrosion. Finally, an area of the nonskid and primer around the scribe was removed with a 2-inch pneumatic die grinder. Sixteen grit aluminum oxide abrasive paper was then used to remove any remaining coating on the substrate. The exposed substrate was then visually inspected for discoloration and corrosion.

Flexibility Test

The nonskid coating was prepared on 6" x 3" x 1/16" flexible primed aluminum panels. Surface preparation involved sanding. To test for flexibility, the nonskid panels were bent over a 5-inch mandrel until cracks appeared in the coating. Ridges of the nonskid profile ran parallel to the axis of the bend. Cracking within a 1/2 inch of the edge was ignored. The degree of bending at which cracking first appeared was recorded. The panels were then bent 20˚ over the mandrel. Cure parameters such as time and temperature were recorded. All the panels were conditioned at room temperature for 24 hours before testing in accordance with ASTM F137.

Coefficient of Friction (COF)

The nonskid was prepared on 12" x 12" x 1/8" primed steel panels. The dynamic COF was measured using the rotating arm meter for dry and wet substrates (μ-Deck Rotating Arm COF Meter) from Vision Point Systems Inc. The test was conducted on two panels. The COF test panel was tested in the as-applied state and was not subjected to nonskid conditioning or wear cycles before testing. The as-applied test panel was subjected to this test procedure under both dry and wet conditions. After completion of the dry condition test, the panels were uniformly wetted with synthetic seawater per ASTM D1141 from a spray bottle until the synthetic seawater ran off the side of the panel surface. The dynamic COF test was performed on each panel immediately after uniform wetting with synthetic seawater. The dynamic COF meter was used in accordance with the manufacturer's directions, and the test procedure was performed. A ball was inserted into the ball holder, and the contact ball was locked into the holder. This was done while ensuring that the surface was in contact with the surface to be measured, which had not been used for a previous measurement. The Vision Point Systems Inc μ-Deck Rotating Arm COF Meter was placed on the test panel to ensure that the ball remained in contact with the surface of the test panel throughout the full 360-degree rotation of the contact ball. The surface temperature (Ts) of the nonskid panel was recorded in degrees Fahrenheit. The Ts of the panel after each COF reading and the uncorrected COF (COFU) were recorded. The temperature corrected COF (COFC) was calculated using the equation COFC = COFU – 0.0048 (75 – Ts). To be considered a pass, the COF must meet the requirements of the MIL-PRF-24667D specification. This calls for minimum dynamic COF values of 1.4 (dry substrate) and 1.1 (wet substrate).

Viscosity was determined by using a TA Discovery HR-2 rheometer. The viscosity (Pa·s) was measured in a flow ramp setting (shear rate from 1 to 100 (1/s)). Initially, the plate height was set to 1550 mm, excess coating removed, and then reduced to 1500 mm to ensure total probe coverage.

FIGURE 4
Unfilled coating after curing (left), and coating filled with fumed silica (right). Both coatings were cured when the substrate was 10 cm below the heater. The wet coating thickness was kept constant (40 mils) through a drawdown bar. Cracking was present in both coatings.

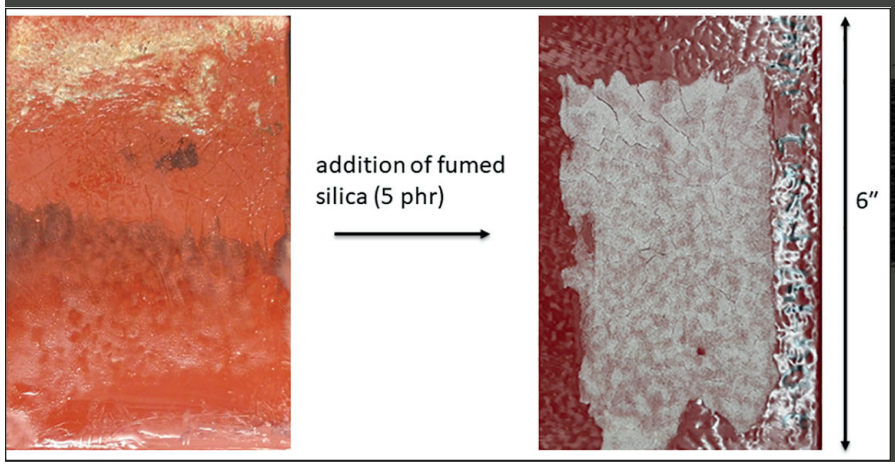

FIGURE 5
Effect of fumed silica loading on cure time of coatings.

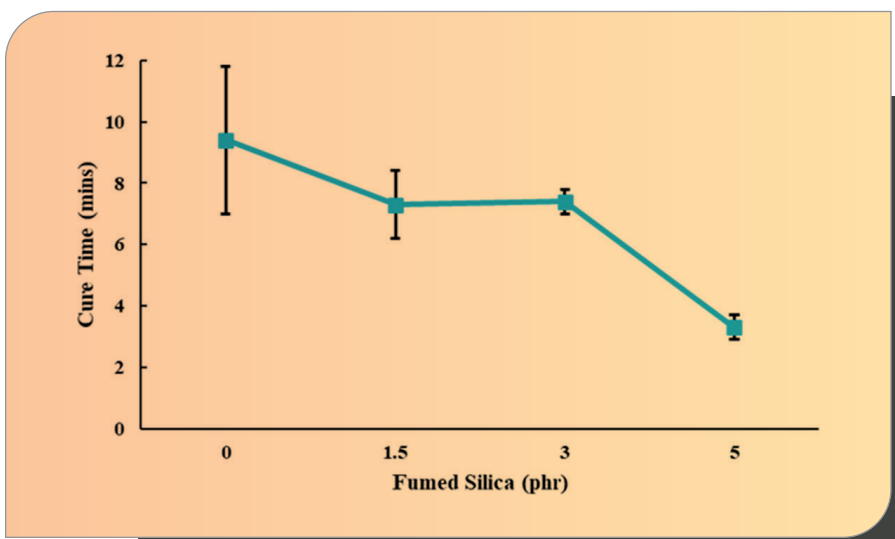

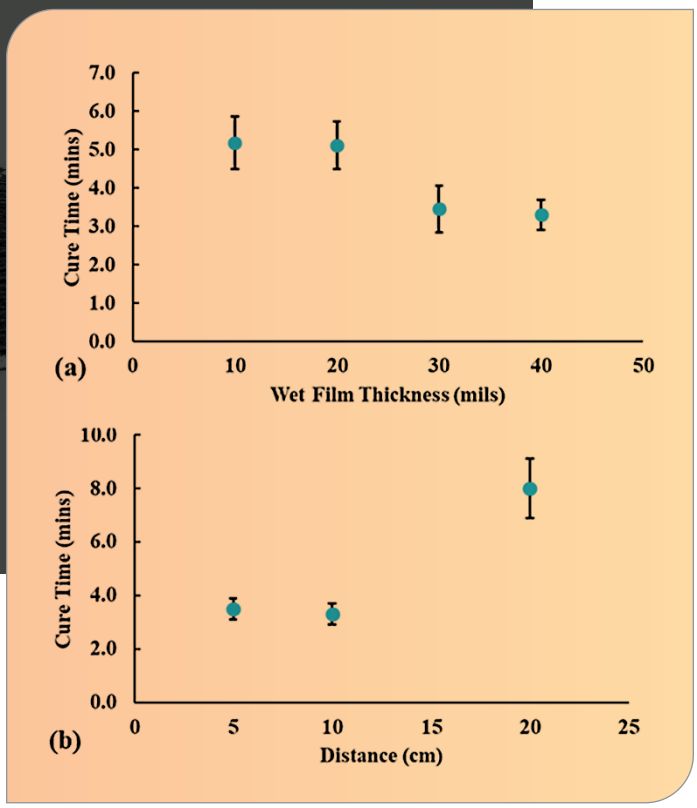

FIGURES 6A-C
Effects of different parameters on the base formulation: (a) effect of coating thickness on cure time and (b) effect of distance between heater and substrate on cure time. The wet film thickness of all coatings is maintained through a drawdown bar (40 mils, unless specified). Each coating was cured while the substrate was 10 cm below the heater except for those in the distance study. Figure 6c shows the coatings formed after curing 5 cm beneath the IR heater. The coating composition consisted of Ebecryl®605 (60 wt %) and PETIA (40 wt %). Luperox®231 (1 phr) and fumed silica (5 phr) were also added.

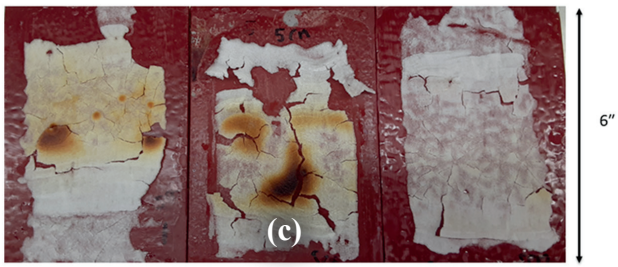

Viscosity was measured for both the non-skid containing aluminum oxide (16 grit, 14 mesh) and base (no aluminum oxide) formulations. Three replicates were tested for each formulation. To determine whether the samples were thixotropic, peak hold experiments were performed at low (1 Hz) and high (10 Hz) shear rates. The first step was at 1 Hz for 60 s, followed by an increase to 10 Hz for 60 s, and returned to 1 Hz for 60 s. Recovery percentage and thixotropy index (TI) were calculated and compared between replicates and formulations with and without aluminum oxide particles.

RESULTS AND DISCUSSION

Base Formulation

The initial formulation consisted of the initiator and resin. As shown in **Figure 4**, convection occurred during curing. The resin would spread and form a thinner coating at the edges. These edges along with other areas required additional time to cure. This formulation could not support a front and overall cure time was in the 10-minute range.

Fumed silica was added to increase the viscosity and eliminate convection. **Figure 5** shows the cure time as a function of fumed silica loading. The results demonstrate that the cure time decreased as the amount of fumed silica increased. Fumed silica (5 phr) was needed to eliminate convection and sustain a front. The average front start time was approximately 2 minutes with a temperature of 105 ˚C on the coating surface. The fronts could not be sustained without constant IR irradiation. Despite this, the generation of fronts significantly reduced cure time. **Figure 4** shows the coating formed after the addition of fumed silica. The coating adheres to the substrate; however, cracking is apparent. These cracks were formed during the curing process and after the coating cooled to ambient temperature. Fumed silica (5 phr) was added to each formulation from this point forward.

Parameters such as wet film thickness, resin concentration, and the distance between the substrate and the infrared heater were studied. The results in **Figure 6a** show that the cure time was lower for the thicker layers (30 and 40 mils). Thinner layers lose more heat due to a higher surface area to volume ratio. In addition, surface tension-driven convection can also arise. The work by Bansal et al. also demonstrates that thinner layers result in lower front velocities.[37] **Figure 6b** shows that the cure time reached a minimum when the heater was 10 cm above the substrate. **Figure 6c** shows that charred and cracked coatings were formed when the heater was 5 cm above the substrate.

Figure 7a shows that the cure time decreased as the relative weight percentage of PETIA to Ebecryl®605 was increased. This result can be explained

FIGURE 7
The effect of the resin composition on (a) cure time and (b) coating appearance. The wet film thickness of all coatings is maintained through a drawdown bar (40 mils). Each coating is cured while the substrate is 10 cm below the heater.

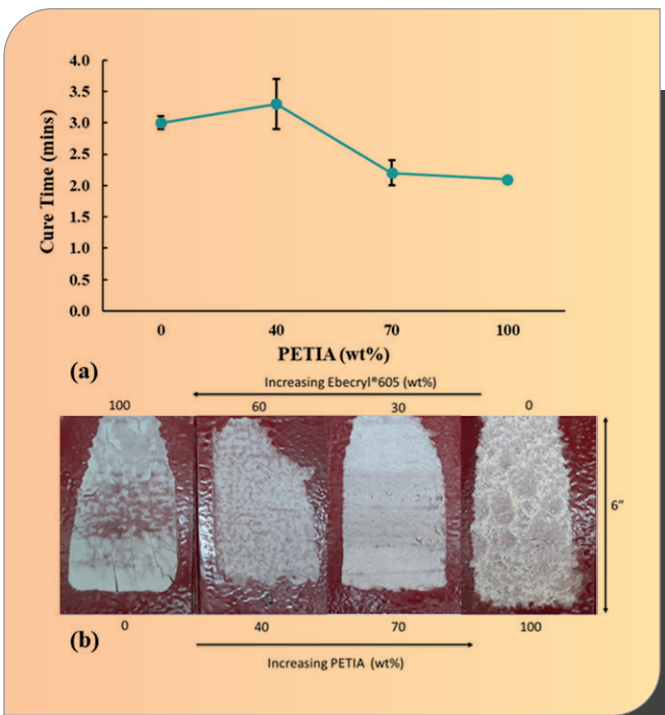

FIGURE 8
The image shows that the addition of milled carbon fiber (20 phr) reduces cracking and forms a nonskid texture.

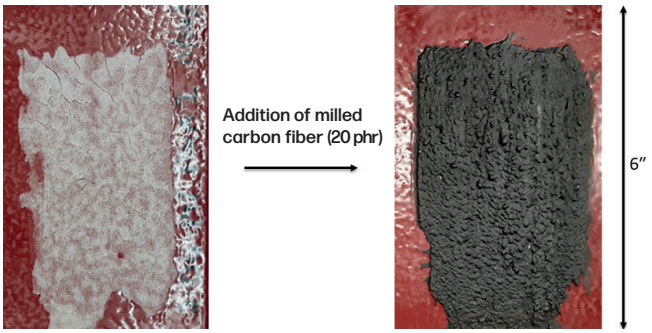

FIGURE 9
Image showing the coatings formed using milled carbon fiber with loadings of (a) 5 phr, (b) 10 phr, and (c) 20 phr.

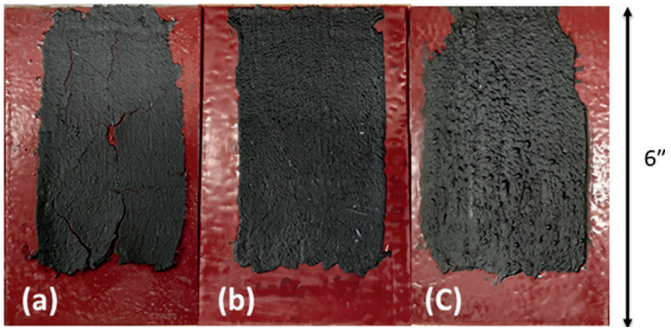

by the higher density of double bonds per molecular weight in PETIA compared with Ebecryl®605. These results align with the findings of Bynum et al. that that front velocity generally increased as the number of double bonds per molecular weight of an acrylate increased.[41] **Figure 7b** shows that the nonskid formulations containing more PETIA formed more brittle and porous coatings while those with more Ebecryl® 605 had large cracks. A resin composition consisting of Ebecryl®605 (60 wt %) and PETIA (40 wt %) was used to optimize cure time while maintaining desirable physical properties.

Parameters such as thickness, fumed silica loading, the distance between the substrate and heater, and resin composition have been optimized. However, cracking remained a challenge.

As shown in **Figure 4**, the base formulation showed significant cracking. According to the Zoltek Corporation, Zoltek®PX35 is a high-aspect ratio filler with a negative coefficient of thermal expansion (CTE, -0.75 x 10^{-6}/K). One of the causes of cracking is due to internal stresses arising from the CTE mismatch between the coating and the steel substrate. Steel has a lower CTE compared with polymer-based coatings; milled carbon fiber is added to reduce the CTE mismatch.[42] As shown in **Figure 8**, the addition of milled carbon fiber (20 phr) to the formulation reduced cracking. **Figure 9** demonstrates that as little as 10 phr of milled carbon fiber is needed to prevent cracking, but the surface of the coating gained a more nonskid texture as more milled carbon fiber was added.

As shown in **Figure 10**, there was a slight increase in cure time as milled carbon fiber was added. The overall average cure time for each loading was relatively similar, in the 3- to 5-minute range. Additional experiments showed that fillers with irregular shapes such as calcium carbonate and kaolin were not able to prevent cracking at the same loading (20 phr) as milled carbon fiber.

FIGURE 10
Effect of milled carbon fiber loading on cure time. The wet film thickness (40 mils) and distance between heater and substrate (10 cm) were kept constant.

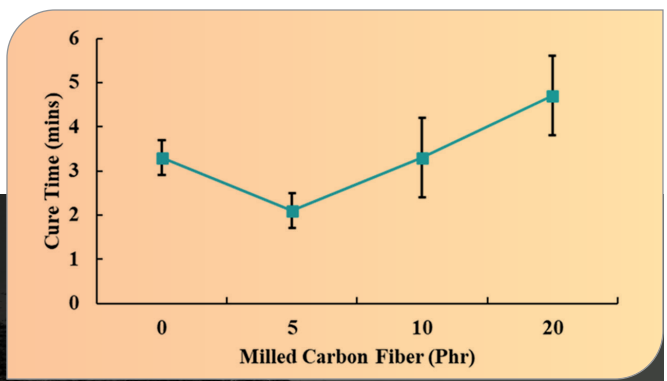

Nonskid Formulation

Preliminary Formulation

Figure 11 demonstrates the curing process of the nonskid formulation. Irradiation with heat ignites a propagating front, which then travels and cures the coating.

FIGURE 11
Image showing propagating fronts as nonskid is being cured under heat.

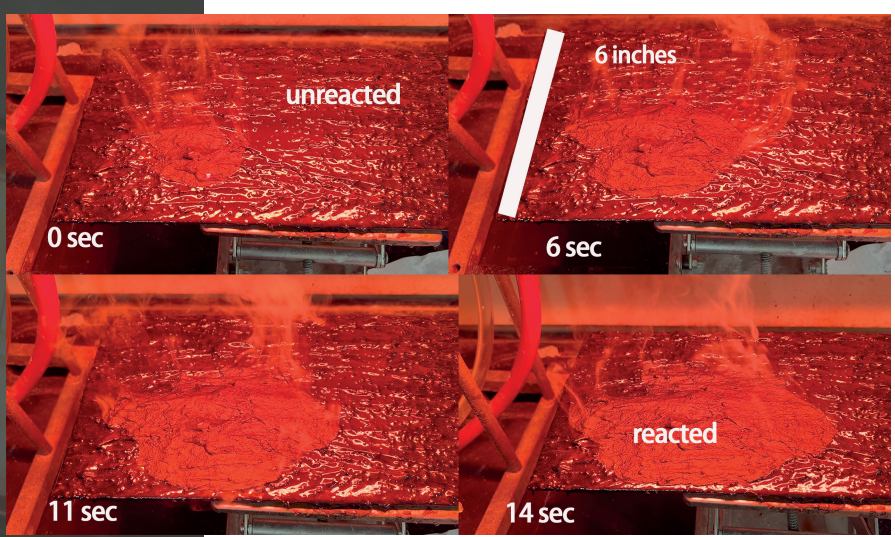

FIGURE 12
Nonskid coating after the addition of 100 phr of aluminum oxide. The nonskid was applied by brush. Note: All other nonskid coatings were applied by roller (20 mm x 75 mm) containing 10 mm grooves.

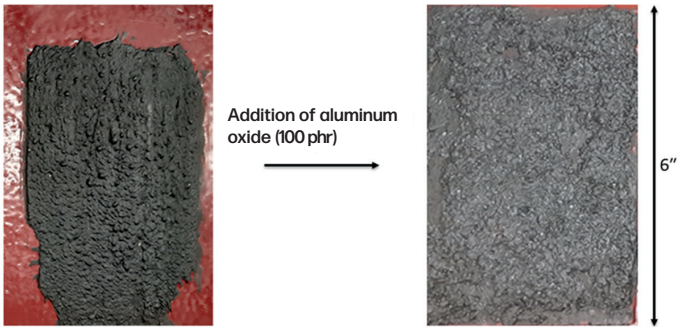

FIGURE 13
Nonskid coatings after impact score with 100 phr of aluminum oxide (top) and 25 phr of aluminum oxide (bottom). The scores were (a) 52.5%, (b) 15%, (c) 77.5%, and (d) 87.5%.

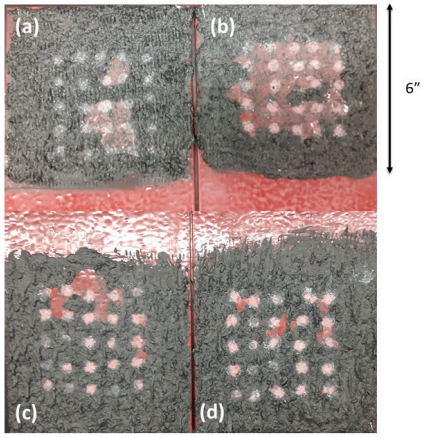

TABLE 1
Cure Parameters for Preliminary Nonskid Coating

FP Start Time (mins)	Temp of Coating Surface at Start of FP (˚C)	Cure Time (mins)	Mass Loss of Resin after Cure (wt %)
1.4	116	8.0	4.8
1.6	115	6.8	4.5
1.5	114	6.8	4.7
1.5 +/- 0.1	115 +/- 1	7.2 +/- 0.7	4.7 +/- 0.2

Through experimentation, it was found that keeping the heater on during the process was necessary to sustain the front. The front does not propagate in the thinner areas of the coating and therefore additional heat irradiation is needed to complete the cure.

Figure 12 shows an image of the cured nonskid coatings while **Table 1** shows the curing data. No cracking or delamination occurred in any of the coatings formed, and an average cure time of around 7 minutes was achieved. The higher cure time in comparison to the base formulation can be explained by the peaks and valleys of the nonskid. As shown in **Figure 6a**, the cure time decreased as the thickness of the film decreased, and this was attributed to heat loss. Heat loss from the resin prevents the propagation of fronts in the thinner areas of the coating. The overall result is that the thicker areas cured more quickly while the thinner areas took longer to cure as no propagating front was generated. This also explains the wider range of cure times in comparison with the base formulation.

To determine the evaporant content released during curing, the difference between the mass of the coating resin before and after curing was determined. It was found that the coating lost approximately 5 wt % of its resin mass (approximately 2 wt % of the total coating mass) after curing. We did not analyze the evaporant, but we speculate that it was composed of resin vapor, volatile impurities in monomer, and byproducts of initiator decomposition.

Impact Testing

The results in **Figures 13a and 13b** demonstrate impact scores of 52.5% and 15%, respectively. This poor and inconsistent performance was attributed to the high loading of the aluminum oxide. This loading led to increased brittleness of the coating and therefore poor impact resistance. To improve impact resistance, the amount of aluminum oxide was reduced from 100 to 25 phr. The results in *Figures 13c* and *13d* demonstrate improved impact scores of 87.5% and 77.5% for nonskid coatings made from formulations containing 25 phr of aluminum oxide.

Two more nonskid coatings loaded with 25 phr of aluminum oxide were treated with synthetic seawater and subsequently tested for impact resistance. These nonskid coatings had no apparent holidays. The nonskid coatings in **Figure 14b** demonstrated comparable impact resistance to the untreated samples. These coatings have consistent impact scores of 87.5% after treatment.

FIGURE 14
The impact scores for the reduced aluminum oxide formulations are comparable between the (a) untreated nonskid coatings and (b) nonskid coatings treated with synthetic seawater (ASTM D1141) for 15 days. The nonskid coatings averaged impact scores of (a) 82.5% and (b) 87.5%.

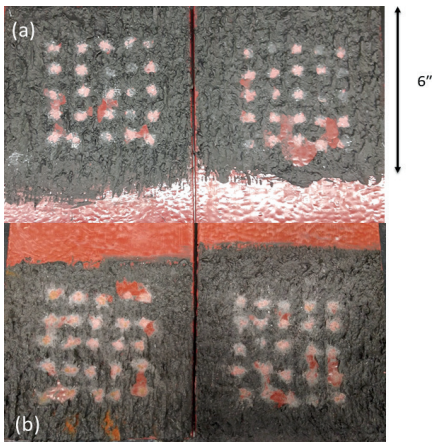

Table 2 shows the various cure parameters for the nonskid coatings loaded with 25 phr of aluminum oxide and applied on panels for impact testing. The table includes temperature parameters such as

TABLE 2
Cure Parameters for Nonskid Coatings Loaded with 25 phr of Aluminum Oxide and Applied in a 6″ x 6″ Area

Initial Substrate Temp (˚C)	Temp of Substrate at Start of FP (˚C)	Substrate Temp at End of Cure (˚C)	FP Start Time (mins)	Total Cure Time (mins)
24	54	167	0.90	5.43
24	58	181	0.97	8.67
22	56	186	0.98	7.08
23	60	165	1.10	7.87
25	61	181	0.93	8.33
22	55	198	0.90	8.42
23 +/-1	57 +/- 3	180 +/- 12	0.96 +/- 0.08	7.63 +/- 1.21

FIGURE 15
Nonskid coatings after the mandrel bending test. (a) Bending until failure (first appearance of cracks). (b) Bending to 20˚.

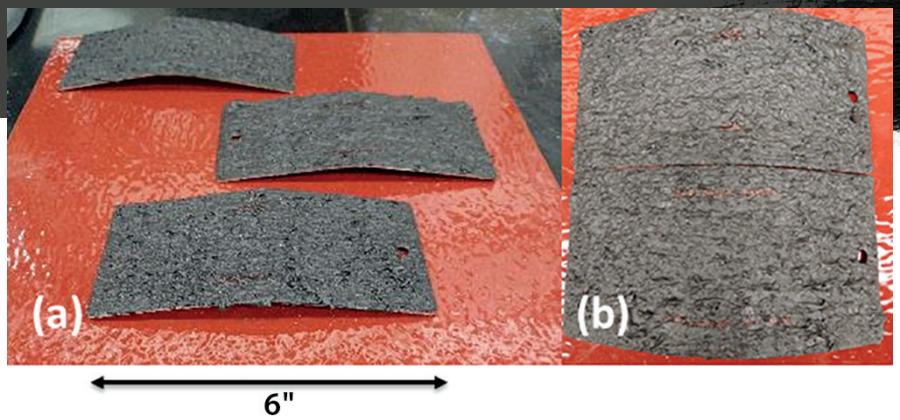

TABLE 3
Cure Parameters for Nonskid Prepared on Panels for the Mandrel Bending Test

FP Start Time (secs)	Temp of Coating Surface at Start of FP (˚C)	Cure Time (sec)
25	115	45
28	114	50
32	117	56
28 +/- 4	115 +/- 2	50 +/- 6

TABLE 4
Results of Qualitative Chemical Testing on Nonskid

Chemical	Time Submerged	Result
Ethanol	24 hours	Pass
Natural seawater	4 weeks	Pass
Detergent	4 weeks	Pass
Deicing-defrosting fluid	24 hours	Pass
Motor oil	4 weeks	Pass

the substrate temperature when FP starts along with the ambient substrate temperature before cure. The time in which FP starts along with the total cure time is recorded. Based on the results, the nonskid started undergoing FP as the surface temperature of the substrate approaches the mid-50s ˚C. By the end of the cure, the temperature of the substrate exceeds 160 ˚C. The cure time varied between 5 and 8 minutes with an average of 7.6 minutes.

Flexibility Testing

The cured nonskid coating on average was able to bend 12˚ before the appearance of cracks. **Figure 15a** shows the bent nonskid coatings. With this flexibility, the nonskid coatings can tolerate a reasonable amount of bend without failure such as cracking or delamination. As shown in **Figure 15b**, delamination is not present even if the coatings are bent 20˚ over the mandrel. Cracking was minor even at these bends. The data in **Table 3** show that the cure time was dramatically lower (less than 1 minute) in comparison with the nonskid applied on the other panels, which can be attributed to a reduction in heat loss to these thinner aluminum panels.

TABLE 5
Results for Coefficient of Friction Testing

Summary	Average COF Dry	Average COF Wet
Panel 1	1.81	1.50
Panel 2	1.80	1.45

Qualitative Chemical Testing

The nonskid coatings showed no delamination or softening upon being submerged in the various chemicals. No differences between such properties were present between the submerged and nonsubmerged areas and the impacted and nonimpacted coating. **Table 4** lists the various chemicals tested. These results demonstrate the good chemical resistance performance of the nonskid. As an example, **Figure 16** shows the result of the qualitative test after being submerged in natural seawater for four weeks. The corrosion present is not a concern as it only occurred in the impact zone and in areas where the coating was not applied.

Corrosion

Figures 17a and **17b** show the nonskid coatings after undergoing the salt-fog test for 1000 hours. Upon inspection, there is no delamination of the nonskid around the scribe, corrosion beyond the scribe, or separation between layers. The results demonstrate the corrosion resistance of this nonskid coating.

FIGURE 17
Images of nonskid coatings after salt-fog testing for 1000 hours.

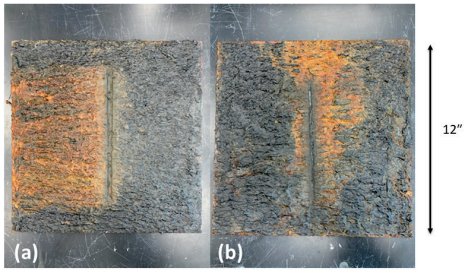

FIGURE 16
Nonskid after submersion in seawater for a month and undergoing the qualitative chemical resistance test.

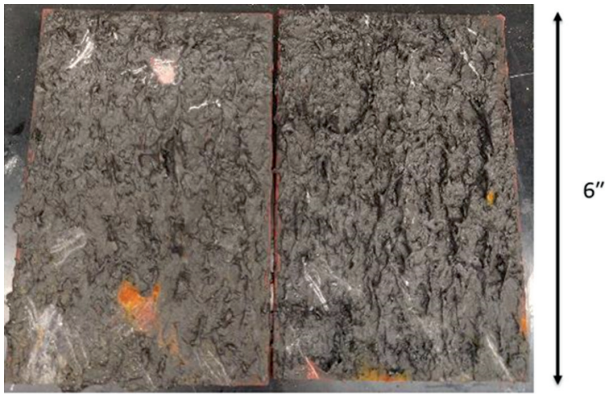

Coefficient of Friction

The specified COF values required are 1.4 (dry) and 1.1 (wet). The results in **Table 5** demonstrate that the nonskid coating exceeds these requirements and allows room for further optimization of the formulation.

Rheology

The results in **Figure 18** present the viscosity with an increasing shear rate for the replicates of nonskid formulations. The fewer number of data points in the nonskid formulation **(Figure 18a)** compared with the base formulation can be attributed to the presence of sharp spikes in the raw viscosity data for the nonskid formulation. These spikes are a result of the aluminum oxide particles contacting the probe. This is further confirmed with sharp spikes in the probe axial force at similar time points during the procedure. To improve the accuracy of the results, the spikes were removed from the data. In the absence of aluminum oxide particles, there are no viscosity spikes in the base formulation, shown in **Figure 18b**. At a low shear rate, 1 (Hz or 1/s), the average viscosities were 302 +/- 44 Pa•s and 475 +/- 40 Pa•s for the nonskid and base formulations, respectively. At a higher shear rate, 10 (Hz or 1/s), the average viscosities were 54 +/- 11 Pa•s and 43 +/- 1 Pa•s for the nonskid and base formulations, respectively.

Figure 19 shows that the formulation is thixotropic. The decrease in viscosity under high shear followed by recovery allows the applicator to easily apply the formulation while also allowing sufficient viscosity recovery for frontal polymerization to occur. **Figure 20** shows that the nonskid and base formulations have an average viscosity recovery of around 60% within 60 seconds of undergoing high shear.

FIGURE 18
The viscosity of coating formulations as a function of shear rate (a) nonskid formulation and (b) base formulation.

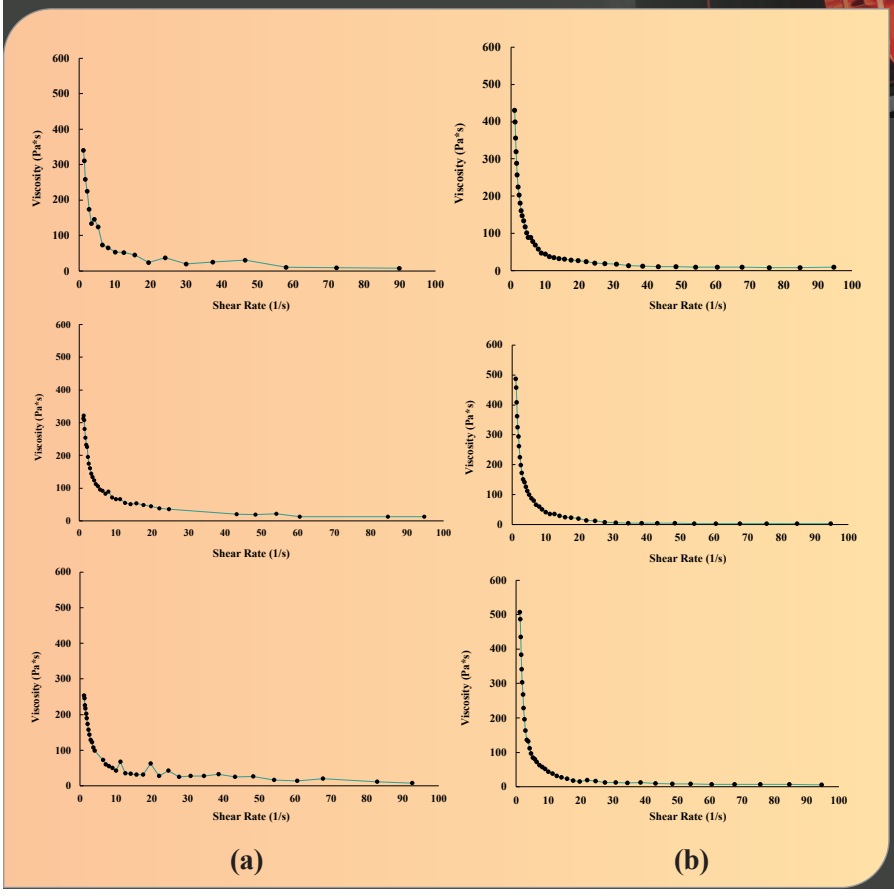

FIGURE 19
Thixotropic behavior of the base and nonskid formulations at low (1 Hz) and high (10 Hz) shear rates.

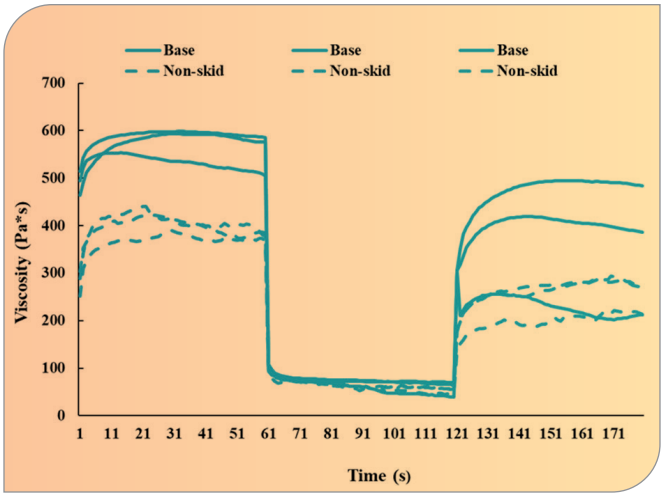

FIGURE 20
The viscosity recovery while undergoing low shear (1 Hz) after undergoing high shear (10 Hz) for 60 seconds.

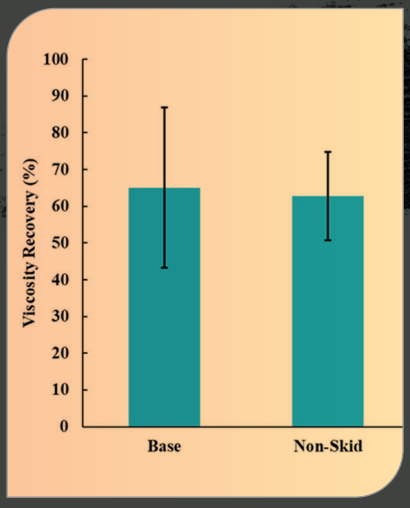

CONCLUSIONS

A novel patent-pending cure-on-demand, nonskid deck coating formulation, consisting of a bisphenol-A epoxy acrylate mixture and PETIA, was optimized for cure time and resistance to chemicals, corrosion, and impact using various fillers. Fumed silica (5 phr) was added to eliminate convection thereby allowing frontal polymerization. Curing of the coating was done by constantly applying heat to generate frontal polymerization. Other parameters such as wet film thickness, resin composition, and distance between the heater and substrate were tested to optimize the coating. Milled carbon fiber was added to eliminate cracking and provide a nonskid appearance.

The resulting base formulation had a cure time in the 5-minute range when applied as a 40 mils-thick coating.

Aluminum oxide was added to the base formulation to provide a desirable nonskid texture. This combination allowed for the development of a cure-on-demand, high-solids nonskid coating for corrosion protection on marine vessels. The coating has an average cure-to-service time in the 7-minute range, and curing starts when the surface of the steel panel exceeds 54 ˚C. The nonskid demonstrated impact resistance in accordance with ASTM G14 with average scores of 82.5% before and 87.5% after treatment in synthetic seawater. Qualified chemical testing demonstrated a wide range of resistance to chemicals such as ethanol and motor oil. The mandrel bend test indicated that the coating will not crack below a bend of 12˚ and delamination does not occur. It was also determined that the nonskid coating will cure more quickly when applied to thinner steel substrates.

Lastly, a salt-fog test in accordance with ASTM B117 demonstrates the corrosion resistance of the nonskid. The current formulation demonstrates promise as a repair coating for nonskid decks on maritime vessels. Further work will be done to improve impact resistance and meet all U.S. Navy specifications. ❊

Acknowledgments

This work was funded by SERDP (GR-000081630). We would like to thank personnel from the Naval Surface Warfare Center, Carderock Division, including Charles White, Kylee Fazende, and Jay Ong. Personnel from Vision Point Systems including Tamara Lubysheva, Matthew Frichtl, and Wayne McGaulley were responsible for the coefficient of friction testing.

Daniel P. Gary, Douglas Ngo, Amber Bui, and John A. Pojman are with the Department of Chemistry and the Macromolecular Studies Group at Louisiana State University in Baton Rouge, LA. Jorge A. Belgodere is with the Department of Biological and Agricultural Engineering at Louisiana State University. Email: john@pojman.com.

References

1. Javadi, A.; Mehr, H. S.; Sobani, M.; Soucek, M. D. *Prog. Org. Coat.* 2016, 100, 2–31.
2. Noè, C.; Iannucci, L.; Malburet, S.; Graillot, A.; Sangermano, M.; Grassini, S. *Macromol. Mater. Eng.* 2021, 306, 2100029.
3. Thanamongkollit, N.; Miller, K. R.; Soucek, M. D. *Prog. Org. Coat.* 2012, 73, 425–434.
4. Chittavanich, P.; Miller, K.; Soucek, M. D. *Prog. Org. Coat.* 2012, 73, 392–400.
5. Sangermano, M.; Cerrone, M.; Colucci, G.; Roppolo, I.; Acosta Ortiz, R. Polym. Int. 2010, 59, 1046–1051.
6. Garra, P.; Dietlin, C.; Morlet-Savary, F.; Dumur, F.; Gigmes, D.; Fouassier, J.-P.; Lalevee, J. *Polym. Chem.* 2017, 8, 7088–7101.
7. Chen, C.; Li, B.; Wang, C.; Iwasaki, S.; Kanari, M.; Lu, D. In *Paint and Coatings Industry*; IntechOpen, 2018.
8. Crivello, J. V. J. *Polym. Sci. Part A: Polym Chem.* 2009, 47, 1825–1835.
9. Salz, U.; Zimmermann, J.; Salzer, T. J. *Adhes. Dent.* 2005, 7, 7–17.
10. Moszner, N.; Salz, U. *Macromol. Mater. Eng.* 2007, 292, 245–271.
11. Baralle, A.; Garra, P.; Morlet-Savary, F.; Dietlin, C.; Fouassier, J. P.; Lalevee, J. *Macromol Rapid Commun.* 2020, 41, e1900644.
12. Chechilo, N. M.; Khvilivitskii, R. J.; Enikolopyan, N. S. *Dokl. Akad. Nauk SSSR.* 1972, 204, 1180–1181.
13. Chechilo, N. M.; Enikolopyan, N. S. Dokl. *Phys. Chem.* 1974, 214, 174–176.
14. Chechilo, N. M.; Enikolopyan, N. S. Dokl. *Phys. Chem.* 1975, 221, 392–394.
15. Chechilo, N. M.; Enikolopyan, N. S. Dokl. *Phys. Chem.* 1976, 230, 840–843.
16. Pojman, J. A. *J. Am. Chem. Soc.* 1991, 113, 6284-6286.
17. Pojman, J. A.; Craven, R.; Khan, A.; West, W. J. *Phys. Chem.* 1992, 96, 7466–7472.
18. Pojman, J. A.; Nagy, I. P.; Salter, C. *J. Am. Chem. Soc.* 1993, 115, 11044–11045.
19. Pojman, J. A.; Willis, J.; Fortenberry, D.; Ilyashenko, V.; Khan, A. J. *Polym. Sci. Part A: Polym Chem.* 1995, 33, 643–652.
20. Pojman, J. A.; Willis, J. R.; Khan , A. M.; West, W. W. J. *Polym. Sci. Part A: Polym Chem.* 1996, 34, 991–995.
21. Khan, A. M.; Pojman, J. A. *Trends Polym. Sci.* (Cambridge, U.K.) 1996, 4, 253–257.
22. Pojman, J.; Fortenberry, D.; Ilyashenko, V. *Int. J. Self-Propag. High-Temp. Synth.* 1997, 6, 355–376.
23. Mota-Morales, J. D.; Gutierrez, M. C.; Sanchez, I. C.; Luna-Barcenas, G.; del Monte, F. *Chem. Comm.* 2011, 47, 5328–5330.
24. Mota-Morales, J. D.; Gutierrez, M. C.; Ferrer, M. L.; Jimenez, R.; Santiago, P.; Sanchez, I. C.; Terrones, M.; Del Monte, F.; Luna-Barcenas, G. *J. Mater. Chem. A*, 2013, 1, 3970–3976.
25. Mota-Morales, J. D.; Gutiérrez, M. C.; Ferrer, M. L.; Sanchez, I. C.; Elizalde-Peña, E. A.; Pojman, J. A.; Monte, F. D.; Luna-Bárcenas, G. J. *Polym. Sci. Part A: Polym. Chem.* 2013, 51, 1767-1773.
26. Fazende, K. F.; Phachansitthi, M.; Mota-Morales, J. D.; Pojman, J. A. *J. Polym. Sci. A Polym. Chem.* 2017, 55, 4046–4050.
27. Washington, R. P.; Steinbock, O. *J. Am. Chem. Soc.* 2001, 123, 7933–7934.
28. Nuvoli, D.; Alzari, V.; Pojman, J.; Sanna, V.; Ruiu, A.; Sanna, D.; Malucelli, G.; Mariani, A. *ACS Appl. Mater. Interfaces* 2015, 7, 3600–3606.
29. Mariani, A.; Bidali, S.; Fiori, S.; Sangermano, M.; Malucelli, G.; Bongiovanni, R.; Priola, A. *J. Poly. Sci. Part A. Polym. Chem.* 2004, 42, 2066–2072.
30. Scognamillo, S.; Bounds, C.; Luger, M.; Mariani, A.; Pojman, J. A. *J. Polym. Sci. Part A: Polym. Chem.* 2010, 48, 2000–2005.
31. Groce, B. R.; Gary, D. P.; Cantrell, J. K.; Pojman, J. A. *J. Polym. Sci.* 2021, 59, 1678–1685.
32. Bomze, D.; Knaack, P.; Koch, T.; Jin, H.; Liska, R. *J. Polym. Sci. Part A: Polym Chem.* 2016, 54, 3751–3759.
33. Xin, Y.; Xiao, S.; Pang, Y.; Zou, Y. *Prog. Org. Coat.* 2021, 153, 106149.
34. Mariani, A.; Fiori, S.; Chekanov, Y.; Pojman, *J. A. Macromolecules*. 2001, 34, 6539–6541.
35. Robertson, I. D.; Yourdkhani, M.; Centellas, P. J.; Aw, J. E.; Ivanoff, D. G.; Goli, E.; Lloyd, E. M.; Dean, L. M.; Sottos, N. R.; Geubelle, P. H.; Moore, J. S.; White, S. R. *Nature.* 2018, 557, 223–227.
36. Lloyd, E. M.; Feinberg, E. C.; Gao, Y.; Peterson, S. R.; Soman, B.; Hemmer, J.; Dean, L. M.; Wu, Q.; Geubelle, P. H.; Sottos, N. R.; Moore, J. S. *ACS Cent. Sci.* 2021, 7, 603–612.
37. Bansal, K.; Pojman, J. A.; Webster, D.; Quadir, M. *ACS Macro Lett.* 2020, 9, 169–173.
38. Pojman, J. A. In *Polymer Science: A Comprehensive Reference*; Matyjaszewski, K.; Möller, M., Eds.; Elsevier BV: Amsterdam, 2012, 957–980.
39. Pojman, J. A. In *Reference Module in Materials Science and Materials Engineering*; Elsevier, 2022, 1–17.
40. Gary, D. P.; Bynum, S.; Thompson, B. D.; Groce, B. R.; Sagona, A.; Hoffman, I. M.; Morejon-Garcia, C.; Weber, C.; Pojman, J. A. *J. Polym. Sci.* 2020, 58, 2267–2277.
41. Bynum, S.; Tullier, M.; Morejon-Garcia, C.; Guidry, J.; Runnoe, E.; Pojman, J. A. *J. Poly. Sci: Part A: Pol. Chem.* 2019, 57, 982-988.
42. Al-Azawi, A.; Cenev, Z.; Tupasela, T.; Peng, B.; Ikkala, O.; Zhou, Q.; Jokinen, V.; Franssila, S.; Ras, R. H. A. *Macromolecular Rapid Communications*. 2020, 41, 1900522.